Effect of Tetraethylene Glycol Dimethyl Ether on Electrical, Structural and Thermal Properties of PVA-Based Polymer Electrolyte for Magnesium Battery

R. Gamal, E. Sheha*, N. Shash and M.G. El-Shaarawy
Physics Department, Faculty of Science, Benha University, Benha, Egypt

(Received July 3, 2014)

The aim of the contribution is to introduce a high performance magnesium conducting polymer electrolytes (PEs) comprising hybrid of poly(vinyl alcohol) (PVA), magnesium bromide ($MgBr_2$) and tetraethylene glycol dimethyl ether (TEGDME) as plasticizer are prepared at various compositions by solution cast technique. X-ray diffraction and thermogravimetric analyses suggest a substantial structural modification, decrease in crystallinity and various interactions in the polymer electrolyte components due to addition of TEGDME. Also there is a marked decrease in T_g with increasing TEGDME. The conductivity conformation with the addition of plasticizer which can be explained on the basis of dissociation of ion aggregates formed in PVA–$MgBr_2$ polymer electrolytes at higher concentrations of the salt. The ionic conductivity of the polymer electrolyte increased with addition of salt and plasticizer reached to the highest conductivity value of $\approx 10^{-6}$ S cm^{-1} at 0.8 ml TEGDME. The frequency dependence of AC conductivity obeys the Jonscher power law. The estimated value of Mg^{+2} ion transference number is found to be 0.68 for high conducting film. The open circuit voltage of a solid state battery which based on the optimum polymer electrolyte with a configuration Mg|PE|V_2O_5 is 1.5 V. Also this battery has exhibited a discharge capacity $\approx$ 3.78 mAh/g. The discharge characteristics are found to be satisfactory as a laboratory cell.

DOI: 10.12693/APhysPolA.127.803
PACS: 77.84.Lf, 72.80.Tm

1. Introduction

The lithium (Li) battery is usually used as a power source because of its high energy density and shape variability. However, high demand for Li battery makes the price of Li grow due to its geographically limitedness in the earth crust [1]. As an alternative to lithium, magnesium has been foregrounded. Magnesium batteries have recently attracted great interest due to their high energy density and environmentally friendly components, safe to handle, coupled with magnesium's low cost ($\approx$\$ 2700/ton for Mg compared to \$64,000/ton for Li) and abundance in the earth's crust ($\approx$13.9% Mg compared to $\approx$0.0007% of Li) [1–4].

But the development of Mg batteries has been hindered by two problems: (1) the kinetically sluggish Mg intercalation and diffusion in cathode materials; (2) the incompatibility between anode and electrolyte due to the high polarizing ability of the divalent Mg^{2+} cation. Thus the search for suitable cathode and less passivated anode/electrolyte configuration is intrinsically urging [5, 6].

Polymer electrolytes (PE) are useful for a variety of electrochemical devices such as batteries, fuel cells, super capacitors, electro chromic devices and chemical sensors [7]. Many aspects of PE can be investigated such as ionic conductivity, nature of films and vibrational properties of functional groups [8]. Generally, PE is ionic conductor which can be obtained by dissolving a salt in a polymer host [8–10].

*corresponding author; e-mail: ISLAM.SHIHAH@fsc.bu.edu.eg

When salts dissolve in a polymer matrix, there are produced ions which serve as charge carriers that contribute to ionic conductivity under the influence of an electric field. Usually, chosen of the salt based on the size of the anions, e.g., $LiClO_4$, NaBr or LiH_2PO_4 [8], but in this work, $MgBr_2$ salt is the doping salt.

The search for magnesium ion conducting polymer electrolytes can be interesting not only for the multivalent cationic conductivity mechanism in the polymer, but also due to their lower cost and ease of handling [11].

PVA is polymer showing excellent properties such as a very high dielectric properties, good charge storage capacity and dopant-dependent electrical and optical properties [12]. It has carbon chain backbone with hydroxyl groups attached to methane carbons; these OH groups can be a source of hydrogen bonding and hence assist the formation of polymer electrolytes [12]. Plasticizers are low in molecular weight, nonvolatile substances (mostly liquids) that, when added to a polymer, improve the flexibility of polymer, increase the process ability, and, hence increase the utility [7]. Plasticizers improve the electrical conductivity of polymer electrolyte by (i) increase the dissociation of salt into ions; (ii) decrease the glass transition temperature of the polymer; (iii) plasticizers associated with the ionic carriers and allowing them to move faster [13] such as ethylene carbonate (EC), polyethylene glycol (PEG), dimethyl formamide (DMF) and (TEGDME). TEGDME was chosen due to its good properties, such as the high boiling point and low volatility, which make it a good choice as electrolyte of batteries [14].

Upon the above considerations, an attempt has been

made to characterize the polymer electrolytes based PVA complexed with magnesium bromide ($MgBr_2$) and TEGDME at different weight percentages to evaluate their physico-chemical performance. In addition, solid-state Mg/PE/V_2O_5 cell was assembled, and it is cycling performances briefly examined to evaluate the applicability of our matrix as an electrolyte to solid-state magnesium batteries. Elemental mapping of V_2O_5 cathode was measured before and after cycling.

2. Experimental

All chemicals used in the present study were received from Sigma Aldrich Chemical Company, Germany. To synthesis $(PVA)_{(1-x)}(MgBr_2)_x$ membrane (M_1), magnesium bromide ($MgBr_2$) with different concentrations, x = 0, 10, 15, 20 and 30 wt%, were added to PVA $(C_2H_4O)_n$ (98–99% hydrolyzed, average MW 88000–97000) and stirred using a magnetic stirrer at 60 °C for 12 h. The prepared solutions were directly cast in a petri-glass dishes and left for ten days at dry atmosphere. $(PVA)_{(0.7)}(MgBr_2)_{0.3}$ membranes (M_2) was the highest conducting polymer electrolyte.

To synthesis $(PVA)_{(0.7)}(MgBr_2)_{0.3}/_{x'}$ TEGDME membrane (M_3), TEGDME with different concentrations, x' = 0, 0.2, 0.4, 0.6, 0.8 and 1 ml was added to M_2 and stirred using a magnetic stirrer at 60 °C for 12 h. The prepared solutions was directly cast in a petri-glass dishes and left for ten days at dry atmosphere. $(PVA)_{(0.7)}(MgBr_2)_{0.3}/_{0.8ml}$TEGDME membrane ($M_4$) was the highest conducting polymer electrolyte. This is illustrated in Fig. 1.

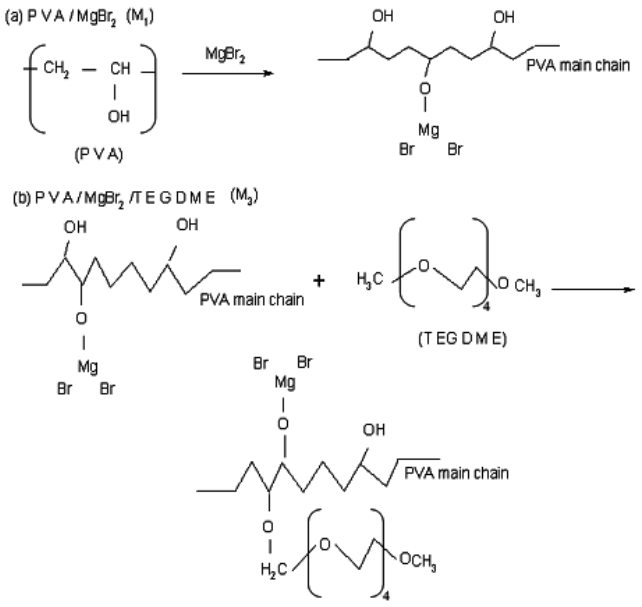

Fig. 1. The scheme for PVA polymer with all addition.

XRD patterns of the films were taken using XRD-6000 Shimadzu diffractometer. The diffraction system was based on Cu tube anode with voltage 40 kV and current 30 mA.

Thermogravimetric analyses (TGA) of the prepared films were carried out using Shimadzu-50 from room temperature to 400 °C with a heating rate of 10 °C/min in nitrogen atmosphere for coaling.

AC conductivity measurements were made by impedance method. Samples of diameter 0.5 cm were sandwiched between the two similar stainless steel electrodes of a spring-loaded sample holder. The whole assembly was placed in a furnace monitored by a temperature controller. The rate of heating was adjusted to be 2 K min^{-1}. Impedance measurements were performed on PM 6304 programmable RCL Philips meter in the frequency ranging from 100 Hz to 100 kHz at different temperatures.

Magnesium transference number (t^{+2}_{Mg}) for M_2 and M_4 films was measured by the steady-state technique which involved a combination of ac and dc measurements. The complex impedance response of the Mg/electrolyte/Mg cell was first measured to determine the cell resistances. It was followed by the dc polarization run, in which a small voltage pulse (ΔV = 0.3 V) was applied to the cell until the polarization current reached the steady-state. Finally, the complex impedance response of the cell was measured again to determine the cell resistance after dc polarization.

A powder mixture of 0.7 g V_2O_5 and 0.3 g graphite powder (QualiKems) was thoroughly ground. Slurry was obtained by mixing 0.2 g $MgBr_2$ and 0.1 g PVA binder using magnetic stirrer hot plate (60 °C) for 2 h. To form cathode pellet, the ground powder was mixed with the slurry and left to cast. The cathode is prepared by cold pressing 0.6 g into a pellet of 13 mm in diameter under 2.5 ton/cm^2. The highest conducting electrolyte was deposited on the cathode substrate with NXG-M1 spin coater at 500 rpm. The anode was prepared by cold pressing 0.6 g magnesium into a pellet of 13 mm in diameter under 2.5 ton/cm^2. Two-electrodes swagelock test cell were assembled, Fig. 2. The cell was charged-discharged at room temperature (at constant time) using multi-channel battery test system (NEWARE BTS-TC35). The current density was 50 μA/cm^2.

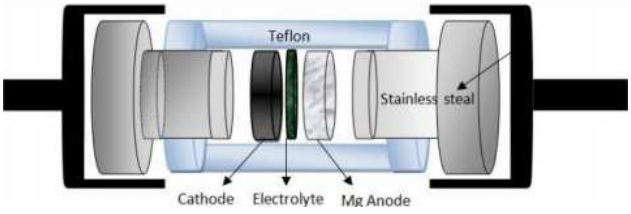

Fig. 2. Schematic design of the lab cell.

3. Results and discussion

X-ray diffraction measurements were performed to investigate the structural properties of the PVA based complexed polymer electrolytes. Figure 3 shows the XRD diffractogram of $PVA_{(1-x)}$ $(MgBr_2)_x/_{x'}$TEGDME membrane (M_5). The broad peak at 20.5° confirms

the semicrystalline nature of pure PVA film. It can be seen that the peak intensity decreased and the band width increased with increase of the concentrations of $MgBr_2$ and TEGDME, which indicates the complete dissolution of the salt in the polymer matrix. The decrease in the intensity of this peak shows that the addition of $MgBr_2$ and TEGDME causes a decrease in the degree of crystallization and causes increase in the amorphous region, which may cause increase of the conductivity and this will be confirmed in conductivity measurement as follows [15].

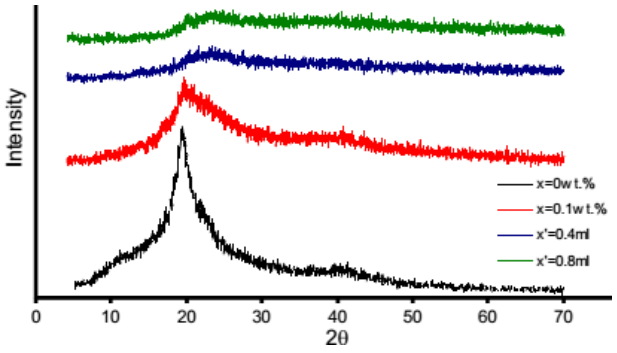

Fig. 3. XRD pattern for M_5 polymer electrolyte.

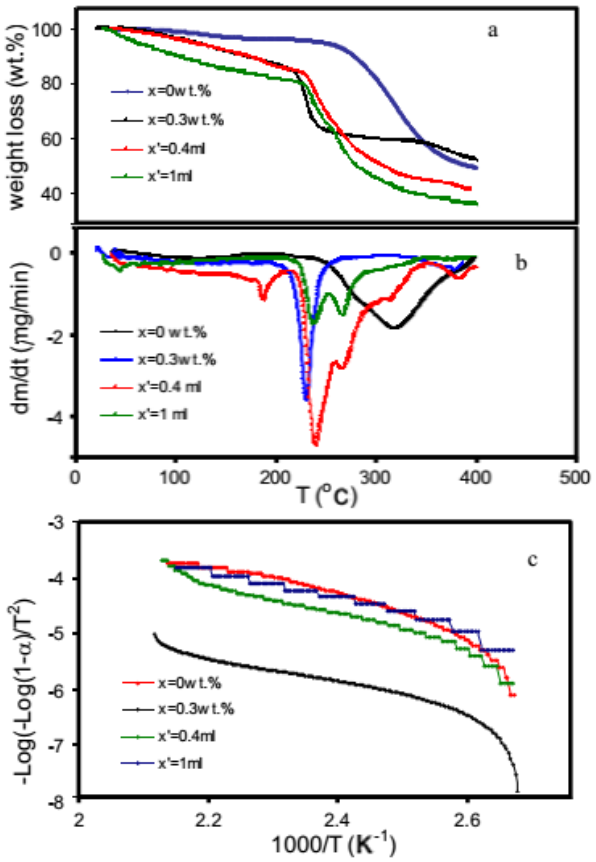

Fig. 4. TGA curves of M_5 polymer electrolyte: (a) weight loss against temperature, (b) derivative of TGA curves, (c) linear plot of TGA curves.

Figure 4 shows weight loss curves as a function of temperature for M_5 from room temperature to 400 °C. From Fig. 4a, it can be seen that the temperature at which the membranes retained 97 wt% of their initial weight decreased from 158.8 °C to 43.69 °C as the salt and plasticizer increased. This may be attributed to difference in the melting point between host, salt and plasticizer. In order to ensure the above findings in detail, the derivative TGA (DrTGA) analysis will be more helpful, Fig. 4b. The glass transition endotherm corresponding to PVA was observed at 114 °C. The peak position shifted to lower temperature with addition of the salt. On the other hand, the glass transition temperature decreased more and more with addition of plasticizer until reached temperature below the room temperature. Decrease of the glass transition temperature causes increase of the segmental motion of the polymer electrolyte. Such segmental motion produces voids, and this enables the easy flow of ions through polymer chains network when there is an applied electric field [16]. The endothermic transformations at 240 °C on DrTGA curve, Fig. 4b, were due to melting temperature (T_m) of the polymer. The melting temperature (T_m) decreased with the addition of $MgBr_2$ and TEGDME which is due to the solvating ability of TEGDME.

Activation energy for the thermal decomposition of the present samples depends on the residual mass and can be calculated using first order integral equation of Coates and Redfern [17]:

$$\log\left(\frac{-\log(1-\alpha)}{T^2}\right) = \log\frac{R}{\Delta E}\left(1-\frac{2RT}{E}\right) - \frac{E}{2.304RT}, \quad (1)$$

where T is the absolute temperature in K, E_a is the activation energy in J/mol, R is the universal gas constant (8.31 J/(mol K)), α is given by

$$\alpha = \frac{w_i - w_a}{w_i - w_f}, \quad (2)$$

where w_a, w_i and w_f are the actual, initial and final weight of the samples, respectively.

By plotting the dependence of $-\log(-\log(1-\alpha)/T^2)$ versus $1000/T$ for each sample, we obtained straight lines, Fig. 4c. The apparent activation energies were calculated from the slopes of these lines using the expression

$$E = 2.303R \times slope. \quad (3)$$

Values of the apparent activation energy, E_a, of the samples are listed in Table I. From this table, it is clear that values of the activation energy are decreased due to addition of $MgBr_2$ and TEGDME but the electrolyte films remain stable in the solid phase over a wide temperature range from 25 to 200 °C, which is advantageous for their potential applications in electrochemical devices.

Figure 5 shows the current–voltage characteristics for M_5 at room temperature. This figure illustrates two regions, one refers to the ohmic region $I \propto V$ and the other region $I \propto V^2$ refers to the formation of space charge region at which the current becomes space charge limited.

TABLE i

Thermal parameters of M_5 polymer electrolyte.

x [wt%]	E_aI [J/mol]	E_aII [J/mol]	T_g	T_m	97% residual weight
0	181.1	64.7	114	240	158.8
30	82.1	53.4	113	215	96.57
$x = 30$ wt%, $x' \approx$ variable					
0.4 ml	58.8	61.6	–	210	89.09
1 ml	50.5	53.1	–	200	43.69

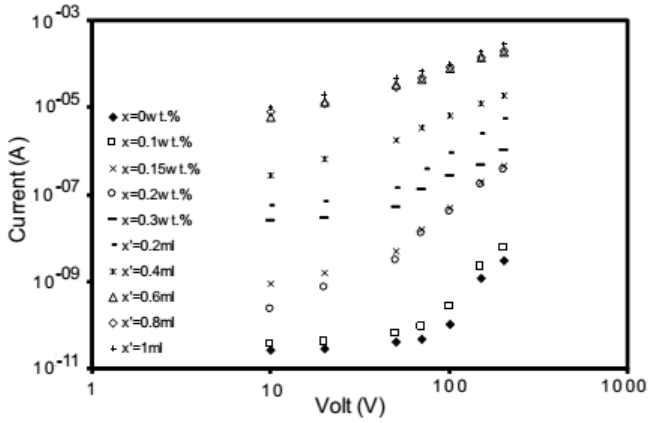

Fig. 5. Current–Voltage characteristics for M_5 polymer electrolyte.

Thus, under high field conditions, the concentration of the free charge carriers injected from electrodes becomes considerably greater than the concentration of thermally generated carriers.

Therefore, the Child–Langmuir law is applicable and the current density J_{sc} given by [18]:

$$J_{sc} \cong 10^{-13} V_{sc}^2 \frac{\mu\varepsilon}{d^3}, \tag{4}$$

where V_{sc} is the applied voltage, μ is the mobility of the charge carriers, d is the sample thickness and ε is the sample permittivity. From this equation we can calculate the values of μ. The ionic conductivity can be expressed as [19]:

$$\sigma = nq\mu, \tag{5}$$

where n is the number of charge carriers and q is the specific charge of the electron $\approx 1.6 \times 10^{-19}$ C. By substituting the values of μ (from Eq. (4)) into Eq. (5), we can obtain the values of n. The values of n and μ listed in Table II. From this table it can be noticed that number of charge carrier and mobility increased with the addition of $MgBr_2$ and TEGDME which attributed to generation of free charge carrier (ions). On the other hand, addition of plasticizer decreases the viscosity which makes a big enhancement in the mobility and increases the dissociation of salt (i.e. produces more free ions). From the slopes of the straight lines in ohmic region $I \propto V$, the ionic conductivity was calculated according to [20]:

$$\sigma_{dc} = \frac{1}{R} \times \frac{t}{A}, \tag{6}$$

where t is the thickness of the polymer electrolyte film and A is the surface area of the film. From Table II, the values of σ_{dc} increased with increase of $MgBr_2$ and TEGDME content. The increase of σ_{dc} was attributed to increase of the mobility and number of charge carriers.

TABLE II

σ_{dc}, number of charge carriers (n) and mobility (μ) of M_5 polymer electrolyte.

x [wt.%]	σ_{dc}	n [C m^{-3}]	μ [cm^2 s^{-1} V^{-1}]
0	1.5×10^{-13}	8.5×10^{11}	9.5×10^{-6}
10	5.3×10^{-13}	1.2×10^{11}	7.3×10^{-5}
15	5.8×10^{-11}	1.7×10^{12}	5.2×10^{-4}
20	7.56×10^{-11}	2.7×10^{13}	1.4×10^{-4}
30	5.8×10^{-10}	9.6×10^{12}	1.3×10^{-3}
$x = 30$ wt%, $x' \approx$ variable			
0.2 ml	8.5×10^{-10}	1.5×10^{14}	1.8×10^{-3}
0.4 ml	1.8×10^{-8}	3.4×10^{14}	1.4×10^{-2}
0.6 ml	4.9×10^{-7}	2.0×10^{13}	1.6×10^{-1}
0.8 ml	4.7×10^{-7}	8.4×10^{12}	4.9×10^{-1}
1 ml	1.3×10^{-6}	4.6×10^{12}	1.8

Figure 6a and b shows the Cole–Cole plot for M_5, at 303 K. The Cole–Cole plot shows semicircle implying equivalent circuit of parallel resistance and capacitance. The plot shows semicircle diameter decrease with increase of the concentration of $MgBr_2$ and TEGDME. The ionic conductivity can be calculated using Eq. (6). The value of R_b (the bulk electrical resistance value) can be calculated from the intercept on the Z' axis.

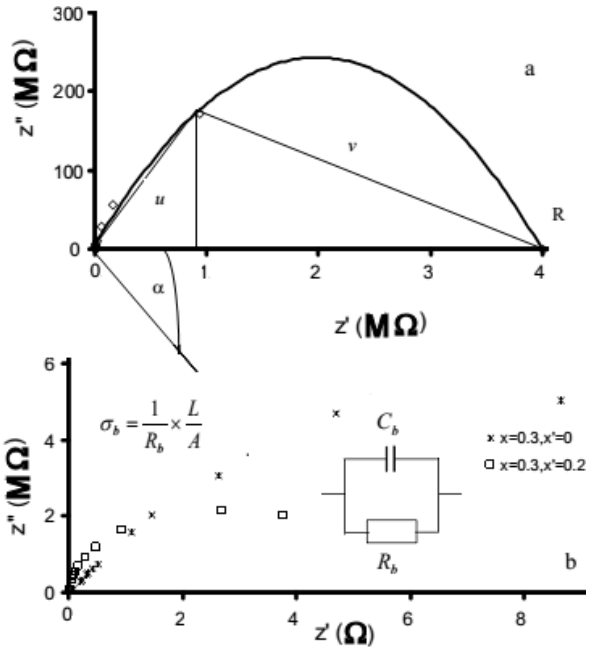

Fig. 6. Cole–Cole plots for M_5 polymer electrolyte where (a) $x = 0$ wt%, $x' = 0$ ml and (b) $x = 30$ wt%, $x' = 0$ ml, $x = 30$ wt%, $x' = 0.2$ ml.

Figure 7a and b shows the bulk conductivity of M_5 as a function of $MgBr_2$ and TEGDME content, respec-

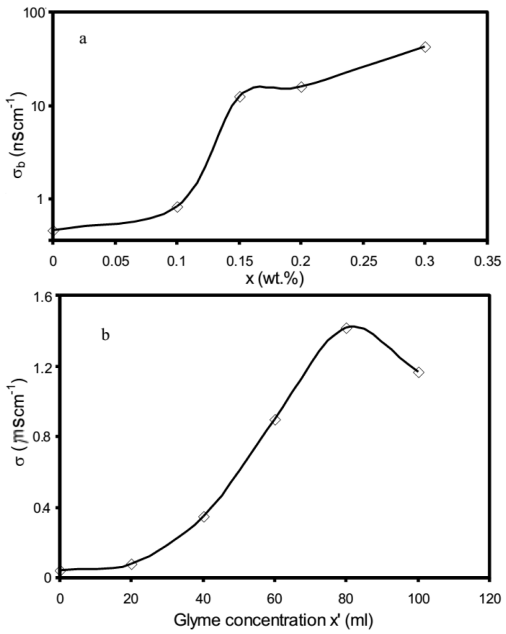

Fig. 7. Variation of ionic conductivity of M_5 polymer electrolyte, (a) $x' = 0$ ml and $x \neq 0$, (b) $x = 30$ wt% and $x' \neq 0$.

tively. The highest conductivity of M_1 polymer electrolyte films was $\approx 10^{-8}$ S cm^{-1} and increased gradually with increase of the weight percentage of TEGDME. The highest conductivity of M_3 polymer electrolyte film is $\approx 10^{-6}$ S cm^{-1} when 0.8 ml TEGDME was added. TEGDME increases the dissociation of salt and thereby produces more free ions and increases the conductivity. This can be attributed to to the plasticizer penetrate the polymer matrix and establish attractive force which can reduce the cohesive forces between the polymer chains. furthermore, the segmental mobility increase [7]. The conductivity decreases beyond $x' = 0.8$ ml of TEGDME. This may be due to fact that the excess amount of TEGDME increases the distance between ions which decrease the conductivity.

The relaxation parameters of the complexes can be obtained from the Cole–Cole plot as shown in Fig. 6. The relaxation time can be calculated from the relation [21]:

$$\frac{v}{u} = (\omega\tau)^{1-h}, \tag{8}$$

where v denotes the distance on the impedance plot between (O, R_b) and an experimental point, u is the distance between the experimental point and (0, 0) and $h = 2\alpha/\pi$ where α is the depressed angle from the z'-axis.

The relaxation parameters are listed in Table III. The relaxation time decreases from $\approx 10^{-3}$ to 10^{-5} s with increase of the concentration of $MgBr_2$ and TEGDME. This can be attributed to that the addition of plasticizer decreases the viscosity of the medium which enhances the mobility of ions, enhancing the mobility of ions leading to decrease of relaxation time and increase of the conductivity which confirmed with conductivity measurement.

TABLE III

Activation energy (E_a), relaxation times (τ) and power (S) of M_5 polymer electrolyte.

x [wt%]	E_aI [eV]	E_aII [eV]	τ [s]	S
0	0.65	0.70	5.27×10^{-3}	0.97
10	0.42	0.78	6.94×10^{-4}	0.88
15	0.48	0.54	7.65×10^{-4}	0.82
20	0.38	0.89	1.59×10^{-3}	0.78
30	0.27	0.78	2.13×10^{-3}	0.69
$x = 30$ wt%, $x' \approx$ variable				
0.2 ml	0.73	–	3.00×10^{-5}	0.73
0.4 ml	0.48	–	5.31×10^{-5}	0.50
0.6 ml	0.32	–	1.04×10^{-4}	0.40
0.8 ml	0.29	0.27	1.22×10^{-5}	0.29
1 ml	0.41	–	1.59×10^{-5}	0.34

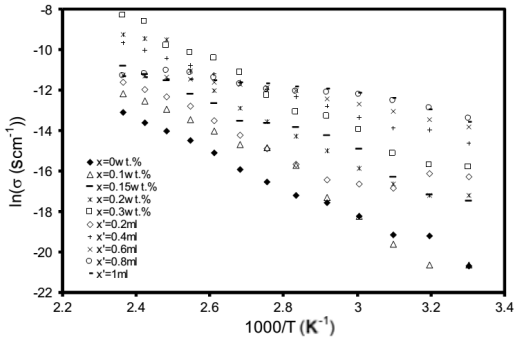

Fig. 8. Temperature dependence of ionic conductivity for M_5 polymer electrolyte.

Figure 8 shows the temperature-dependent ionic conductivity of M_5. From the plot it is evident that, as temperature increases, the conductivity also increases for all systems. The increase in conductivity with temperature has been explained in terms of segmental motion that result in increase of free volumes of the sample and the motion of ionic charge. The conductivity can be expressed as [22]:

$$\sigma = \sigma_0 \exp(-E_a/k_B T), \tag{8}$$

where σ_0 is the pre-exponential factor, E_a is the energy of activation for conduction, K_B is the Boltzmann constant and T is the temperature in K. As shown in Fig. 8, the data are fitted well into two different thermal regions. Activation energy at different concentrations of $MgBr_2$ and TEGDME was obtained using fitting of Eq. (8). Table III presents the activation energy data; it can be observed that the lowest activation energy is for the film doped with 0.8 ml TEGDME, which indicate that TEGDME have effect on $Mg^{2+}Br^-$ dissociation and ionic transfer.

Figure 9 shows the frequency-dependent conductivity of M_5. The plot shows two regions: The first region observed at low frequency plateau region corresponds to the frequency independent conductivity (σ_{dc}). The second region observed at the high frequency dispersion region which corresponds to the conductivity increases with increase of frequency. This behavior obeys the universal

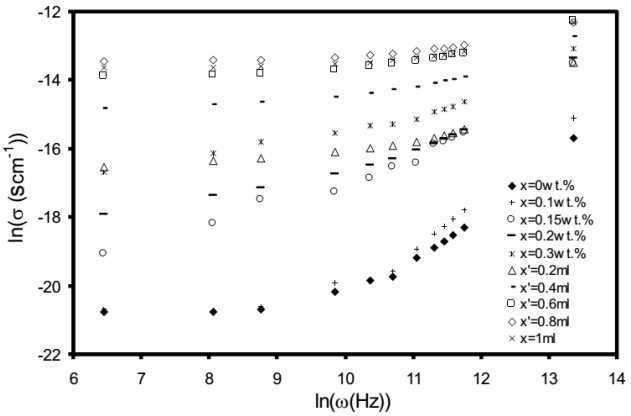

Fig. 9. Frequency dependence of ionic conductivity for M_5 polymer electrolyte.

power law [23]:

$$\sigma_{\rm tot}(\omega) = \sigma_{\rm dc} + A\omega^n, \tag{9}$$

where $\sigma_{\rm dc}$ is the dc conductivity (the extrapolation of the plateau region to zero frequency), A is the pre-exponential factor, ω is the angular frequency and n the fractional exponent which lies between 0 and 1. According to the jump relaxation model, at low frequencies, ions can jump from one site to its neighbouring site. While at higher frequencies, due to the short time periods, the probability for ions to go back to their initial sites increases which causes increase in the conductivity [24].

The values of the exponent n have been obtained using the least square fitting of Eq. (9); it can be observed that the exponent n decreases with increase of concentration of salt and plasticizer.

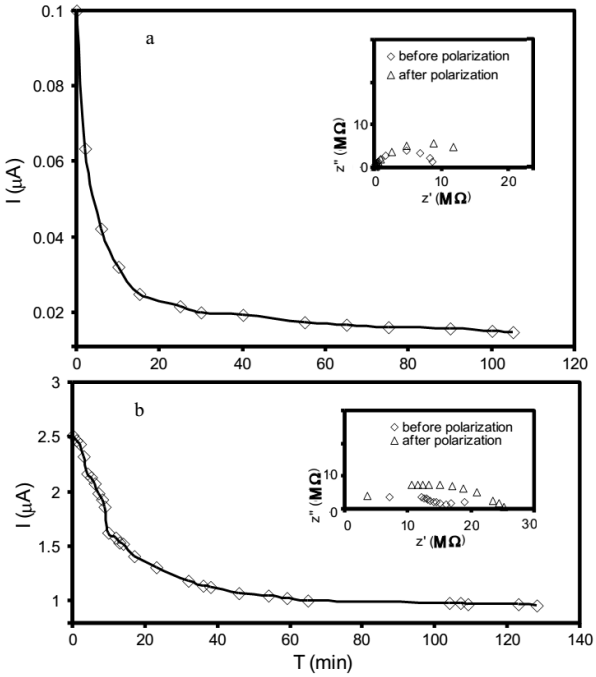

Fig. 10. The variation of polarization current as a function of time for (a) Mg/M_2/Mg and (b) Mg/M_4/Mg cell.

Figure 10a and b shows the current relaxation curve for M_2 and M_4, respectively. The impedance spectra were obtained before and after the polarization of Mg/M_2/Mg and Mg/M_4/Mg cell. The magnesium transference number $t_{\rm mg}^{2+}$ was measured by the following equation [25]:

$$t_{\rm mg}^{2+} = \frac{I_{\rm s}\left(\Delta V - R_0 I_0\right)}{I_0\left(\Delta V - R_{\rm s} I_{\rm s}\right)}, \tag{10}$$

where I_0 and $I_{\rm s}$ are the initial and final steady-state currents and R_0 and $R_{\rm s}$ are the cell resistances before and after the polarization, respectively. The values of $t_{\rm mg}^{2+}$ obtained for M_2 and M_4 polymer electrolytes are 0.56 and 0.68, respectively.

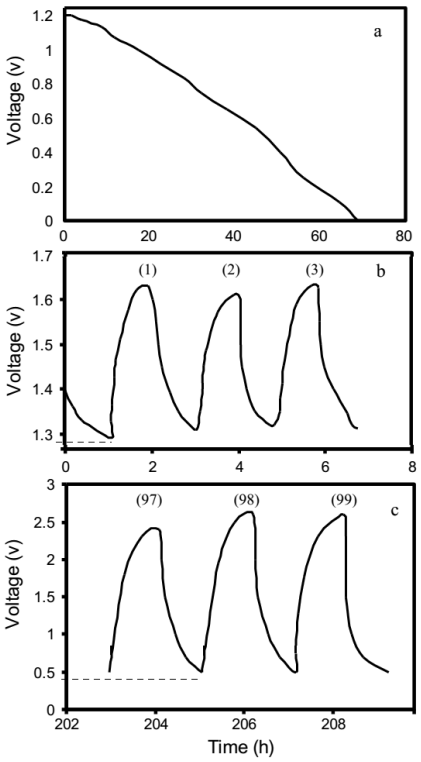

Fig. 11. Discharge characteristics of Mg/M_4/V_2O_5 cell (a) complete discharge curve, (b, c) charge–discharge cycles.

The film with the highest ionic conductivity was used for cell fabrication. Figure 11a shows the complete discharge curve of the battery, it shows that the discharge was sustained for 68 h. The value of the discharge capacity C was evaluated from the equation [26]:

$$C = \int_0^t I(t)dt \tag{11}$$

by integrating the area under the curve of Fig. 11a. The discharge capacity was estimated by 3.78 mAh. Figure 11b,c shows cycling voltage against time of Mg/M_4/V_2O_5 cell. From this figure, it can be noticed that the discharge cycling voltage decreased with increase of cycling. This may be due to large interfacial resistance between the electrodes and the electrolyte which is aggravated during cycling [27].

TABLE IV

EDX results of V_2O_5 cathodes before and after cycling.

Elements	Original electrode	Electrode after the first discharge	Electrode after the first charge
	[at %]		
C	65.18	56.98	58.84
O	18.9	25.71	24.3
Mg	1.31	6.77	4.73
V	7.02	4.39	6.5

Figure 12a–c shows the morphological effect of the electrochemical process on V_2O_5 cathode. The relevant EDS spectrum was printed at the bottom of each image. From these figures, the cathode surface became smooth after cycling compared to the rough surface of the pristine electrode (before cycling). The EDS spectrum indicates the ratio of V, O and Mg elements and the data are illustrated in Table IV. The table indicated that the ratio of Mg increased after cycling. Increasing of Mg means that the electrolyte allows the flow of Mg ions, from anode to cathode [27].

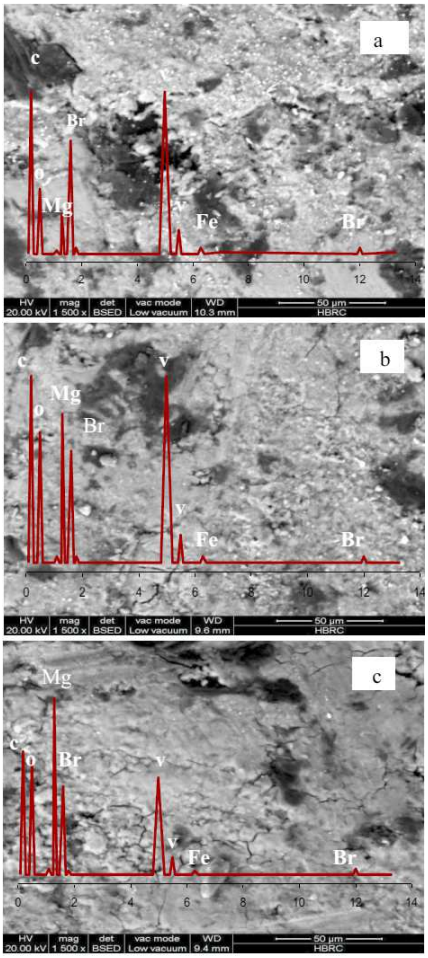

Fig. 12. SEM images of the V_2O_5 cathodes: (a) pristine, (b) after cycling, and (c) after complete discharge. EDS patterns are presented in the images (overlapped).

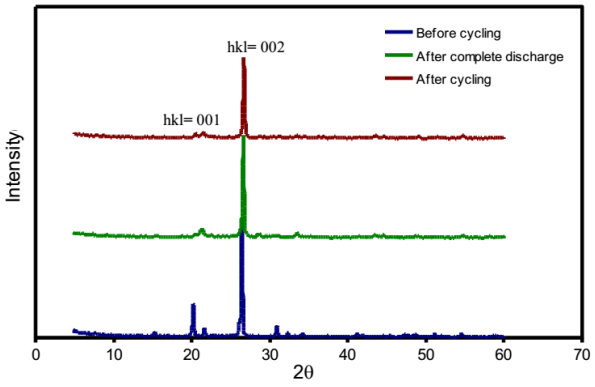

Fig. 13. XRD pattern of V_2O_5 cathode, before and after cycling.

Figure 13 shows XRD pattern of the cathode before and after cycling. The data correspond an orthorhombic phase with preferentially oriented (001) plane and this peak matched quite well with JCPDS file No. 65-0131 for V_2O_5. The intensity of this plane is attenuated and broadened after cycling. This can be attributed to the substitution of Mg^+ with V^+ ions and this agrees with the EDS results.

The particle size of the cathode before and after cycling was calculated from X-ray data using the Scherrer equation [28]:

$$D = 0.9\lambda/(B\cos\theta), \tag{12}$$

where 0.9 is the Scherrer constant, λ is the wavelength of X-ray, B is the breadth of the pure diffraction profile and θ is the incidence angle of the X-ray. These results are listed in Table V. This reduction in the crystallite size after cycling can be attributed to the strain experience due to the intercalation of Mg^{+2} within V_2O_5 [29].

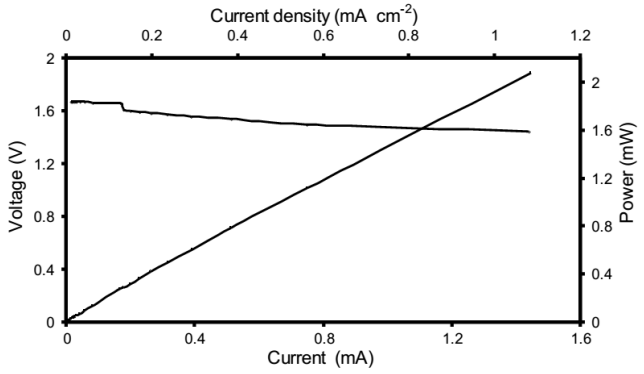

Fig. 14. $I-V$ and $J-P$ curves for $Mg/M_4/V_2O_5$ cell.

Figure 14 shows the current–voltage ($I-V$) and current density–power density ($J-P$) characteristic curves for the $Mg/M_4/V_2O_5$ battery at room temperature. $I-V$ curve had a simple linear form which indicated that the polarization on the electrode was primarily dominated by ohmic contributions. The internal resistance of the battery was obtained from the gradient of the $I-V$ curve $\approx$185 Ω. The plot of the operating $J-P$ suggests

that the contact between electrolyte/electrodes was good. The voltage of the battery dropped to a short circuit current density of 1.085 mA cm^{-2} and the maximum power was determined to be 2.07 mW.

TABLE V

XRD results of V_2O_5 cathodes before and after cycling.

V_2O_5	2Θ	d	FWHM	Particle size [nm]
original	20.22	4.39	0.197	39.93
after the first charge	21.5	4.13	0.236	31.29
after the first discharge	21.44	4.15	0.157	47.21

4. Conclusions

The results are summarized as follows:

- The ionic conductivity of the PE depends on the content of $MgBr_2$ and TEGDME.
- The highest conductivity of the polymer electrolyte examined was 1.42×10^{-6} S/cm (at 30 °C) for M_4 polymer electrolyte.
- The enhancement in ionic conductivity when adding TEGDME to M_2 complex might be due to the role of that dissociation of the Mg salt results in an increase in the concentration of mobile carriers and mobility.
- EDS and X-ray study of the cathodes before and after cycling showed that the electrolyte allowed the flow of Mg ions.
- TEGDME played a key role in enhancement of the Mg^{2+} ion transport number. The maximum value of t^{2+}_{Mg} is found to be 0.68.

References

[1] J. Park, J.S. Kim, J.W. Park, T.H. Nam, K.W. Kim, J.H. Ahn, G. Wang, H.J. Ahn, *Electrochim. Acta* **92**, 427 (2013).

[2] D. Lv, T. Xu, P. Saha, M.K. Datta, M.L. Gordin, A. Manivannan, P.N. Kumta, D. Wang, *J. Electrochem. Soc.* **160**, 351 (2013.

[3] B. Peng, J. Liang, Z. Tao, J. Chen, *J. Mater. Chem.* **19**, 2877 (2009).

[4] W.Y. Li, C.S. Li, C.Y. Zhou, H. Ma, J. Chen, *Angew. Chem.* **45**, 6155 (2006).

[5] Y. Liu, L. Jiao, Q. Wu, J. Du, Y. Zhao, Y. Si, Y. Wang, H. Yuan, *J. Mater. Chem. A* **1**, 5822 (2013).

[6] D. Aurbach, Z. Lu, A. Schechter, Y. Gofer, H. Gizbar, R. Turgeman, Y. Cohen, M. Moshkovich, E. Levi, *Nature* **407**, 724 (2000).

[7] P.C. Sekhar, P.N. Kumar, A.K. Sharma, *IOSR J. Appl. Phys.* **2**, 1 (2012).

[8] N.E.A. Shuhaimi, L.P. Teo, S.R. Majid, A.K. Arof, *Synth. Met.* **160**, 1040 (2010).

[9] M. Forsyth, S. Jiazeng, D. MacFarlane, *Electrochim. Acta* **45**, 1249 (2000).

[10] Z. Gadjourova, Y.G. Andreev, D.P. Tunstall, P.G. Bruce, *Nature* **412**, 520 (2001).

[11] A.R. Polu, A. Kumar, *Bull. Mater. Sci.* **34**, 1063 (2011).

[12] E. Sheha, H. Khoder, T.S. Shanap, M.G. El-Shaarawy, M.K. El Mansy, *Optik* **123**, 1161 (2012).

[13] T. Winie, A.K. Arof, *J. Appl. Polym. Sci.* **101**, 4474 (2006).

[14] M. Marinaro, S. Theil, L. Jörissen, M.W. Mehrens, *Electrochim. Acta* **108**, 795 (2013).

[15] V. Aravindan, G. Kathikaselvi, P. Vickraman, S.P. Naganandhini, *J. Appl. Polym. Sci.* **112**, 3024 (2009).

[16] J. Malathi, M. Kumaravadivel, G.M. Brahmanandhan, M. Hema, R. Baskaran, S. Selvasekarapandian, *J. Non-Cryst. Solids* **356**, 2277 (2010).

[17] E.M. Abdelrazek, I.S. Elashmawi, S. Labeeb, *Physica B* **405**, 2021 (2010).

[18] W.Y. Yan, L.Y. Ai, X.J. Song, G.G. Rui, *Chin. Phys. B* **21**, 8 (2012).

[19] G.K. Prajapati, R. Roshan, P.N. Gupta, *J. Phys. Chem. Solids* **71**, 1717 (2010).

[20] M.R. Johan, O.H. Shy, S. Ibrahim, S.M.M. Yassin, T.Y. Hui, *Solid State Ion.* **196**, 41 (2011).

[21] F. Salman, S. Abo-Elhssan, E. Sheha, M.K. Elmansy, *Turk. J. Phys.* **28**, 57 (2004).

[22] G.K. Prajapati, P.N. Gupta, *Physica B* **406**, 3108 (2011).

[23] A.K. Jonscher, *Nature* **267**, 673 (1977).

[24] H.M. Ahmad, S.H. Sabeeh, S.A. Hussen, *Asian Trans. Sci. Technol.* **1**, 16 (2012).

[25] S. Panero, B. Scrosati, H. Sumathipala, W. Wieczorek, *J. Power Sources* **167**, 510 (2007).

[26] E. Sheha, M.K. El-Mansy, *J. Power Sources* **185**, 1509 (2008).

[27] B.M. Abdel-Samiea, A. Basyouni, R. Khalil, E. Sheha, H. Tsuda, T. Matsui, *J. Mater. Sci. Eng.* **678**, 10 (2013).

[28] S.A. Mohamed, A.A. Al-Ghamdi, G.D. Sharma, M.K. El Mansy, *J. Adv. Res.* **5**, 79 (2014).

[29] E. Sheha, M. Nasr, M.K. El-Mansy, *Mater. Sci. Technol.* (2015).